THOR 5TH PERCENTILE FEMALE ATD DESIGN

Zhenwen Wang, Joseph McInnis, Leonard Benfant and Zhaoying Feng
Humanetics Innovative Solutions, Inc.
USA

Ellen Lee
National Highway Traffic Safety Administration
USA

Paper Number 17-0295

ABSTRACT

The National Highway Traffic Safety Administration (NHTSA) contracted the development of the THOR (**T**est **D**evice for **H**uman **O**ccupant **R**estraint), an advanced frontal impact 50th percentile male Anthropomorphic Test Device (ATD), i.e. THOR-50M. The THOR-50M ATD incorporates substantial improvements in biofidelity and measurement/injury prediction capability compared to the current Hybrid III 50th dummy in NHTSA regulation. Because the available data demonstrates that safety concerns for small females differ from those of mid-sized males, the THOR 5th Percentile Female ATD (THOR-05F) is now being designed to provide improved biofidelity compared to the Hybrid III 5th Female ATD.

This paper presents the latest design of the THOR-05F ATD being developed. This THOR-05F design, while based on the THOR-50M design concepts, also includes changes and new concepts to the head, neck, shoulder, thorax, abdomen, pelvis, and extremities. In general, these changes are incorporated in order to improve the manufacturability and usability of the dummy, to better comply with the most up to date anthropometry specifications, and also to meet updated biofidelity requirements.

Design changes to the THOR-05F head and neck were incorporated to improve manufacturability and usability. The shoulder structure was redesigned to meet the anthropometry specifications and reduce the complexity for manufacturing, while retaining the appropriate joint configuration and range of motion. A range of motion limiter was added to the design of the lower thoracic spine pitch adjustment joint to prevent the dummy upper torso from falling over during assembly/disassembly and pitch adjustment operation. Abdomen pressure sensors were designed into the dummy to replace the abdomen IR-TRACCs, to address potential durability issues for the expected use of the small female dummy (e.g. in a rear seat environment), and to provide an alternative way to predict submarining and abdomen injury. The pelvic bone was designed in accordance with a statistical representation of a 5th percentile female pelvis, resulting in more accurate anthropometry compared with the Hybrid III 5th female pelvis. The arms were redesigned to better represent the human anthropometry and the flesh cutout cavity for bone insert was reduced to minimize the metal bone joint exposure. The leg design was revised to improve its anthropometry and handling. A molded shoe was integrated into the foot design to minimize the mechanical response variance of the shoes purchased from the market. Accommodations for optional in-dummy DAS were included in the ATD design. Finite element analysis was carried out for the ankle joint to optimize the design. In addition, lessons learned from THOR-50M program were taken into considerations throughout the design process.

In conclusion, this paper presents the design of a new THOR-05F dummy being developed to address the safety needs of the small female population. Prototype fabrication, biofidelity evaluation, and certification testing are planned and results will be presented in the future.

INTRODUCTION

The National Highway Traffic Safety Administration contracted development of the THOR, an advanced frontal impact 50th percentile male ATD (THOR-50M). The THOR-50M ATD incorporates substantial improvements in biofidelity and measurement/injury prediction capability compared to the current Hybrid III 50th percentile male ATD in NHTSA regulation. Following the THOR-50M, the development of a small female ATD to predict and mitigate frontal impact injuries to small female occupants was undertaken. Statistical study of injuries in the field shows that female injuries differ from a male due to the female's small size and low mass, which changes how the female interacts with restraint systems (Bose et al 2011, Kahane 2013 and Parenteau et al 2013). Specifically, females have a higher risk of belt and airbag sourced injuries (Parenteau et al 2013). In order to reduce the injury risk for the small female occupant, an advanced small female ATD known as the THOR 5th percentile female (THOR-05F), based mainly on the design concepts introduced in the THOR-50M, is being developed.

The first THOR-05F prototype was fabricated and tested more than a decade ago (McDonald et al 2003). No additional changes were made to the dummy since that time. Though, many improvements have been incorporated into THOR-50M. In September 2015, NHTSA awarded Humanetics Innovative Solutions (referred as Humanetics thereafter) a contract to build three THOR-05F female ATDs with improvements adopted in the THOR-50M. This paper describes the resulting THOR-05F design.

METHODS

Reed et al 2013 compared the anthropometry of current ATDs with the US adult population. The UMTRI AMVO 5th percentile female (Robbins 1983) represents the stature and body mass 151 cm and 48.2 kg, which is very close to the current civilian average 5th percentile female with 151 cm stature and 50.3 kg body weight. Although the body weight increased by 2.1 kg, UMTRI AMVO 5th is still the most representative anthropometry data for automotive occupants, and was selected as the primary anthropometry specification for this dummy design. Autodesk Inventor was used for THOR-05F CAD design. The complex flesh geometry was developed with Geomagic®, converted to Autodesk Inventor format and assembled in the THOR-05F CAD design. The designs were finalized through discussions between Humanetics and NHTSA and all final decisions were made by NHTSA. Body segment mass, center of gravity and mass of moment inertia were measured in Autodesk Inventor against the design specification.

RESULTS

THOR-05F design is summarized in this section, including head, neck, thorax/shoulder, abdomen, pelvis, arms, legs and feet.

Head Design

The head design is similar in concept to the THOR-50M. The skull and the facial plate were combined to reinforce the structure (See Figure 1).

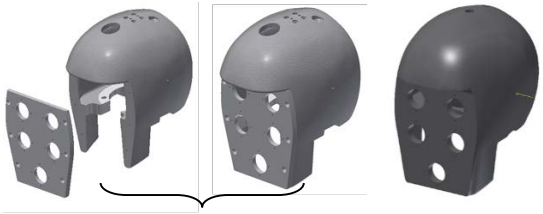

THOR-50M concept THOR-05F

Figure 1. THOR-05F head design

The THOR-05F design has three linear accelerometers at the head center of gravity location and three angular velocity sensors aligned with the head coordinate orthogonally (See Figure 2). In addition, three redundant linear accelerometers were designed in the head as options for the users. A tilt sensor is also included.

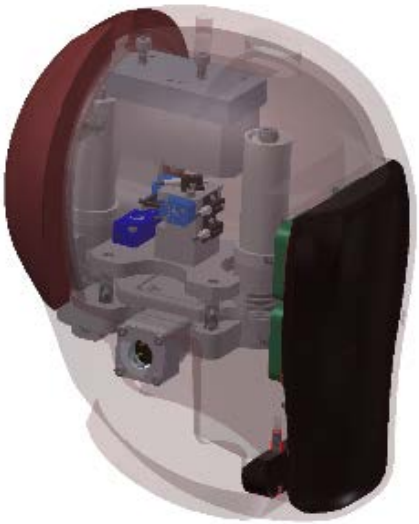

3 linear accels, 3 ARS & 3 redundant linear accels

Figure 2. THOR-05F head sensor configuration

Neck Design

The neck design concept differs from THOR-50M, and has been described previously as the "beta neck" (Martin et al 2009). Instead of having a concentric rubber segment, the design was laid out in a "stairway" style, with elliptical rubber elements of varying cross-sections (See Figure 3).

Figure 3. THOR-05F neck design

The upper and lower neck load cells were redesigned to improve manufacturability. The lower neck load cell still offers the same handling ability in assembly/disassembly as THOR-50M, i.e. the load cell can be removed without disassembling the whole neck. It provides the users convenience to remove the load cell for calibration or swap out load cells when necessary. The T1 accelerometer block was designed to be in the mid-sagittal plane (See Figure 4) to avoid the offset mounting location in THOR-50M.

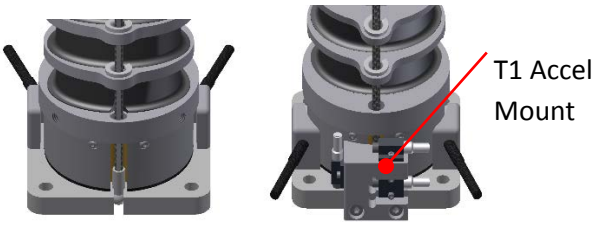

Front View Rear View

Figure 4: Lower neck load cell design

A few other minor changes were implemented in the THOR-05F head-neck interface. These changes include integrating the neck spring cable retainer into the neck spring tube, replacing the

rear roller custom-made pin with a standard shoulder bolt and implementing the tilt sensor mount into the top neck bracket (See Figure 5).

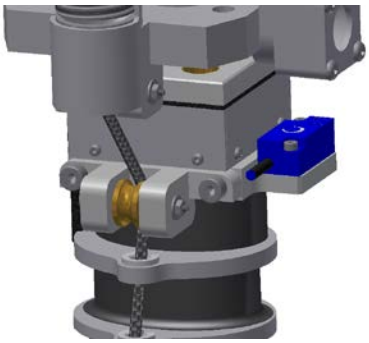

Figure 5. THOR-05F head-neck interface design

Shoulder Design

Clavicle geometry was critical for vehicle shoulder belt engagement from the THOR-50M test experience. The clavicle geometry defined for the THOR-05F was based on the statistical shape model of the clavicle developed by Lu et al 2013 (See Figure 6).

Figure 6. Overlay of THOR-05F clavicle and statistical shape model defined in Lu et al 2013.

The shoulder design uses the same concept as THOR-50M SD-3 that was presented by Lemmen et al 2013. The geometry of the components was simplified to reduce the manufacturing complexity. A one-piece shoulder pad was designed to improve the continuity and coupling with the shoulder skeletal structure (See Figure 7). The shoulder pad is made of a thermoset plastic material that is very durable.

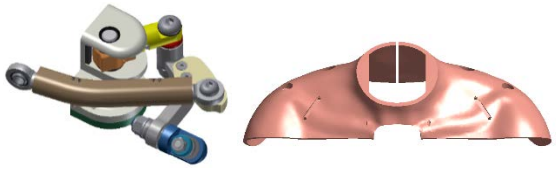

Left shoulder joint Shoulder pad

Figure 7. THOR-05F shoulder design

Upper Extremity

A humanlike shoulder joint offset was introduced into the humerus design to address the "jamming" effect between upper arm and the lateral side of the chest - upper arms were pushed outward because of the incorrect upper arm bone position in the arm flesh. The anthropometry and the THOR-05F design is shown in Figure 8.

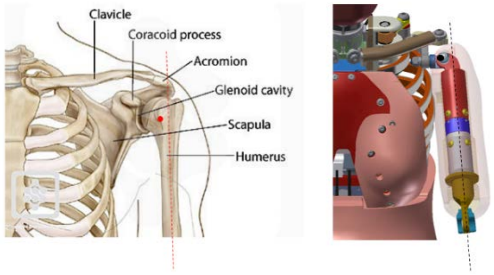

Figure 8. THOR-05F humerus design

The Hybrid III and THOR-50M have the elbow joint at the center of the elbow surface shell, which is not humanlike. The elbow joint was redesigned to have the elbow pivot joint located to the UMTRI AMVO 5th percentile female elbow joint landmark, which is close to the bottom of the elbow, while maintaining the structure of the elbow within the AMVO 5th shell.

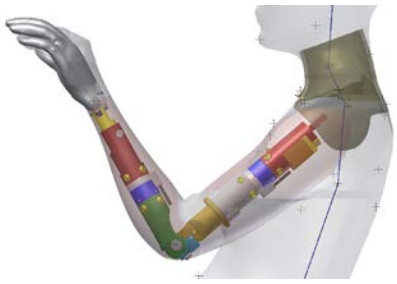

Figure 9. THOR-05F elbow joint design

Thorax Design

The ribcage design concept is similar to THOR-50M with seven ribs. The bottom four ribs are configured parallel at 52.9 degrees relative to the back of the torso, which was derived from Kent et al 2005. The upper three ribs were spaced to cover the cavity (Figure 10).

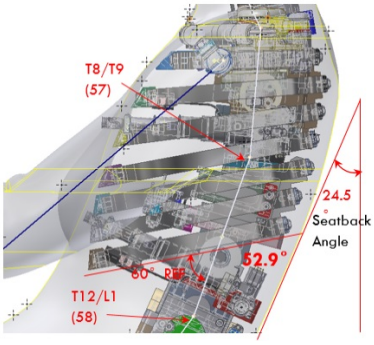

Figure 10. THOR-05F ribcage layout

Tylko et al 2006 showed that the breast position has significant influence on the interaction between chest jacket and shoulder belt in the Hybrid III 5th ATD. To address the breast location variance in testing, the sternum and the breast were integrated together to improve the repeatability of the breast position in assembly (See Figure 11). The sternum is made of hard plastic and the breast is made of soft polyurethane. The thorax will be covered by a neoprene jacket, similar to the THOR-50M, with no foam inserts or pockets.

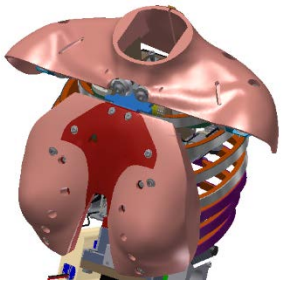

Figure 11. THOR-05F sternum/breast design

Range of motion limiters (See Figure 12), were added to the lower spine joint design, which are intended to prevent the dummy upper torso from falling over in assembly/disassembly and pitch adjustment operation.

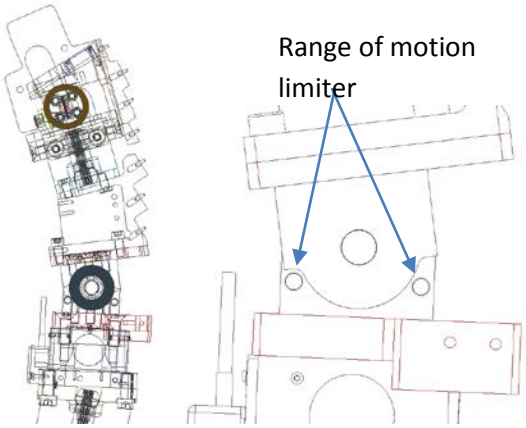

Figure 12. Lower spine joint range of motion limiter

Pelvis Design

A statistical 5th percentile female pelvis model was recently developed by Klein et al (2016a, 2016b). The study provides geometry for the small female predicted using a new statistical pelvis model that is parameterized by age, body mass index and bispinous breadth (See Figure 13). This new pelvic bone geometry was integrated into the UMTRI AMVO 5th percentile female in CAD by aligning the hip joints and

visually best match the anterior superior iliac wing (ASIS) landmarks (See Figure 14).

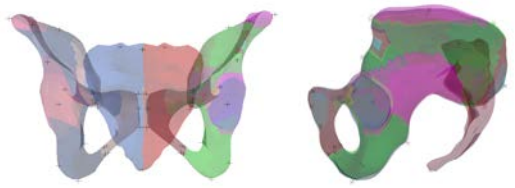

Figure 13. Statistical pelvis model generated by Klein et al (2016a, 2016b)

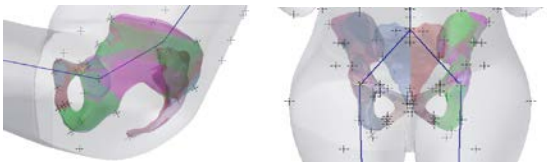

Figure 14. Pelvic bone model and UMTRI AMVO 5th percentile integration

The ATD pelvic bone design was modeled to follow the geometry of this female bone geometry. Material was added to the inner cavity of the pelvic ring to reinforce the pelvic bone for strength requirement in ATD testing and the outer geometry is preserved.

The pelvis flesh geometry in the UMTRI AMVO study is in a compressed condition. However, an uncompressed pelvis flesh is desired for ATD design. Todd et al 1994 studied the buttock compression for patients sitting in wheelchair. A finite element model was developed to predict the flesh compression in such condition. The model was validated with volunteer data in supine position. The predicted female buttock tissue compression is approximately 30 mm in the seated position.

When the buttock flesh is compressed, the pelvis bulges and its breadth becomes wider than that in the uncompressed condition. To estimate the uncompressed pelvis breadth for UMTRI AMVO 5th female, the pelvis breadth ratio between the compressed and uncompressed conditions is desired, but not available. The ratio between the standing and sitting hip breath from ANSUR 1988 data (Gordon et al 1998) was used to derive the ratio. The ratio was then applied to UMTRI AMVO to calculate the uncompressed pelvis breadth. The pelvis breath of ANSUR 1988 in sitting posture represents the compressed condition, and that in standing posture represents the uncompressed condition. It is assumed the bulging ratio in ANSUR and UMTRI AMVO are similar. The uncompressed pelvis flesh for the THOR-05F ATD was developed with this derived target pelvis breadth and compression.

Table 1. Pelvis breadth estimation for uncompressed pelvis flesh

	ANSUR 1988	**UMTRI AMVO**
Compressed	Sitting 366.8 mm	Sitting 380 mm
Uncompressed	Standing 341.8 mm	Standing (calculated) 356 mm

Abdomen Design

Abdomen Pressure Twin Sensors (APTS) were originally developed for the Q dummies (EEVC Report 2016). The development showed that the pressure sensors can be used as alternative to predict the abdomen injuries and submarinning together with the Anterior Superior Iliac Spine (ASIS) load cells. These are being implemented in the THOR-05F design (See Figure 15). In addition, replacing abdomen IR-TRACCs with APTS sensors will eliminate potential damage to the IR-TRACCs if subjected to large magnitude abdomen compression under lap belt loading during submarining. APTS sensors were designed for submarining prediction and are durable under this type of loading.

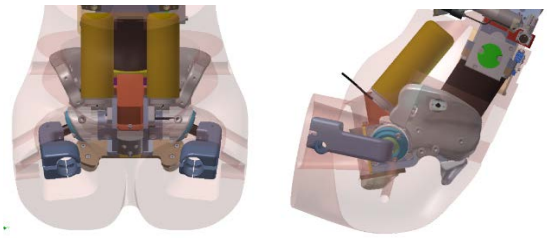

Figure 15. Abdomen pressure twin sensors design in THOR-05F

Abdomen design was split into upper and lower abdomen to facilitate the assembly/disassembly of the sensors and abdomen. The steering wheel and rigid bar probe impact locations for biofidelity/qualification tests were reviewed to ensure the impact does not occur at any gap or split (See Figure 16).

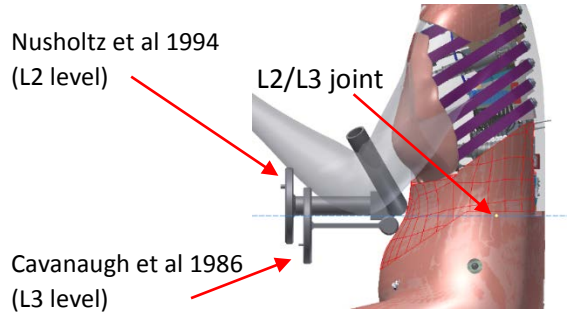

Figure 16. THOR-05F upper and lower abdomen split line (upper abdomen has grids in red color). Impact locations for various biofidelity/ qualification tests are called out.

Knee Thigh Complex

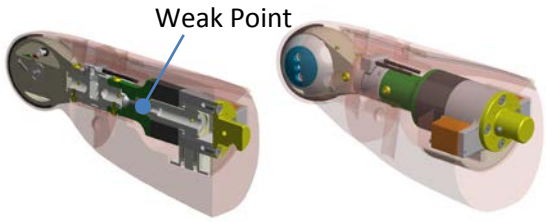

Figure 17 THOR-05F Knee Thigh Complex Design

The knee thigh complex design is similar to the THOR-50M (see Figure 17). The plunger of the compression element in THOR-50M design failed in severe test conditions (See Figure 18). The rubber compression element assembly orientation was flipped to place the weak point closer to the knee (small bending arm yields smaller bending moment when loaded at knee) to mitigate the failure. The stress analysis shows the current design would survive at the load higher than the femur load cell capacity.

Figure 18 Failure of THOR-50M femur plunger shaft

The knee design is the same as THOR-50M.

Lower Extremity Design

The original FLX (Shams et al 2002) was developed prior to 2002 and was never a scaled down version of the THOR-50M leg (THOR-LX). Following the design of the FLX after 2002, NHTSA identified issues with repeatability, durability and reproducibility. Since that time, considerable attention has been given to updating the THOR-50M leg, but no revisions have been made to the original FLX design. Therefore, in conjunction with the current design of the THOR-05F, it was desired to substantially revise the FLX design to incorporate lessons learned from the THOR-50M leg. The design presented in this paper reflects the knowledge gained from THOR-LX efforts. The THOR-05F lower leg design has the same concept as THOR-50M. It was repackaged to fit into the UMTRI AMVO 5th percentile anthropometry. The shoe was derived from the scanned geometry of MIL Specification 7.5W female shoe used in Hybrid III 5th ATD. A new foot bone was shaped to better represent a human metatarsal

(Figure 19). An optional instrumentation package with tilt sensors, angular rate sensors, and accelerometers were designed into the ATD foot (See Figure 20).

Figure 19. THOR-05F foot bone shape

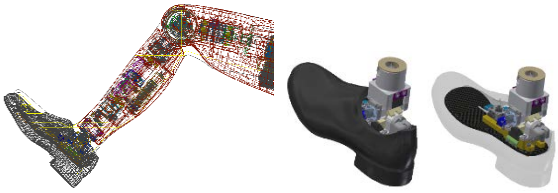

Figure 20. THOR-05F leg and foot design

The Achilles spring damper system was restructured so that it is a standalone module for assembly (See Figure 19). The attachment screws are oriented in an angle that allows disassembly of the whole module as a unit. Two sets of accelerometer mounting holes were designed into the tibia to accommodate the most commonly used accelerometers. The upper tibia bumper was integrated into knee clevis to meet the anthropometry requirement.

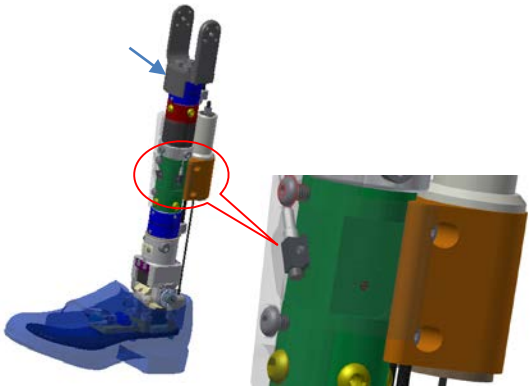

Figure 21. Tibia design featuring Achilles spring damper system (right)

Ankle Joint Simulation

A finite element (FE) model was developed and used to analyze the response of the ankle joint and optimize the mechanical design. In the analysis, the torque cylinder contribution, bumper shape, material stiffness and rubber friction were studied to find a combination that has the best biofidelity. In all analyses, the range of motion of the ankle joint was prescribed as the input. The biofidelity of THOR-05F inversion and eversion was scaled from specifications defined in Funk et al 2002.

Torque cylinder analysis

The THOR-50M design has torque cylinders, which consist of four round rubber rods, which are compressed into the corners of cavities formed by an outer square housing and a shaft with square end (See Figure 20).

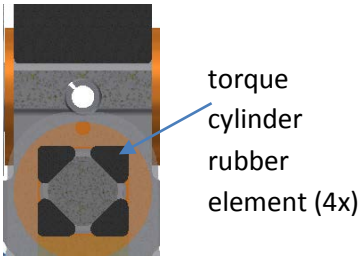

Figure 22. Torque cylinder design around the pivot shaft of the ankle joint

FE analysis was carried out with and without the torque cylinder. It was shown that the torque cylinder contribution to the ankle joint response was insignificant for both eversion and inversion (See Figure 21 and Figure 22, respectively). Based on this analysis, the torque cylinder feature was removed to reduce the ankle design complexity.

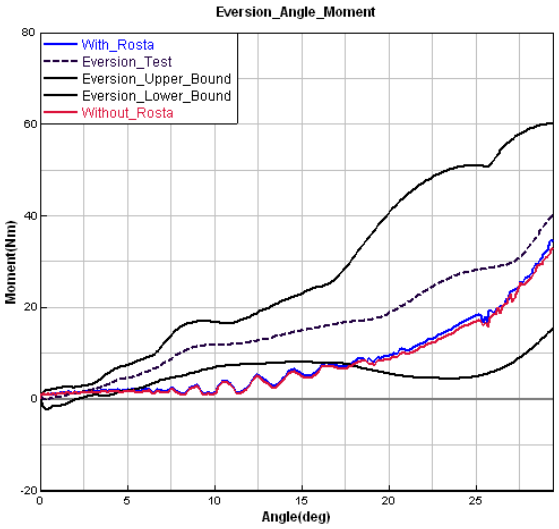

Figure 23. Eversion moment vs rotation comparison with and without torque cylinder, overlaid upon the upper and lower bound of the biofidelity corridor

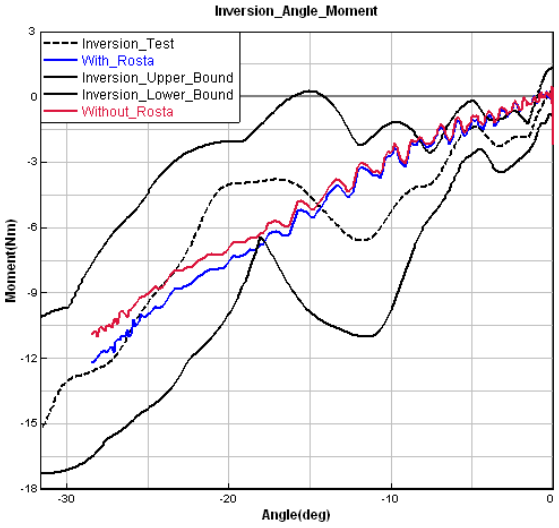

Figure 24. Inversion moment vs rotation comparison with and without torque cylinder, overlaid upon the upper and lower bound of the biofidelity corridor.

Ankle bumper analysis

The FE analysis was conducted for the ankle bumper design. Two materials were used for the analysis (See Figure 23).

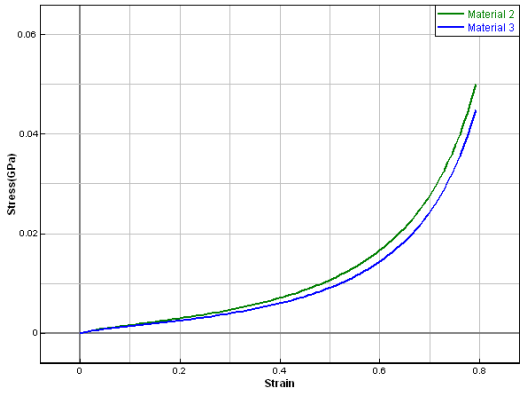

Figure 25. Material properties used for the bumper design analysis

The FE analysis showed the original bumper shape design has high local stress and it bottoms out at 25 degrees in inversion and 30 degrees in eversion, shown in Figure 24 and Figure 25 respectively.

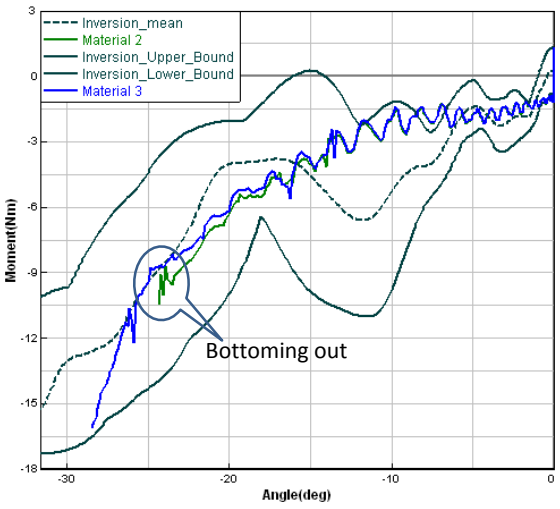

Figure 26. Inversion response of ankle finite element analysis

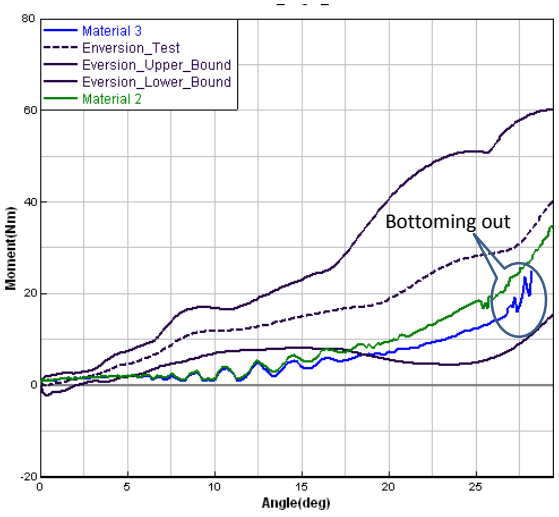

Figure 27. Eversion response of ankle joint finite element analysis

In addition, it was noticed that the original ankle bumper was pushed out and contacted the potentiometer housing (See Figure 26).

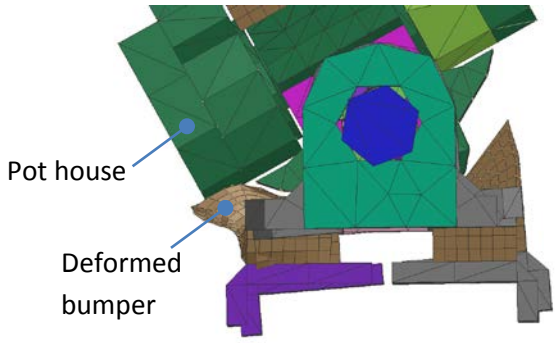

Figure 28. Bumper contacts the pot housing in ankle joint inversion rotation of the original ankle design

Ankle Joint Design

To address the issue observed from the analysis, the ankle joint was redesigned to 1) eliminate high local strain in the ankle bumpers by redistributing the strain evenly in the new bumper design 2) remove the torque cylinder, which has insignificant contribution to the ankle stiffness, and 3) to reduce the size of the ankle mechanical design to better conform to anthropometry specifications. To eliminate the localized high strain, a radial bumper (See Figure 27), was designed so that the strain will be uniform throughout the bumper when compressed. Due to the removal of the torque cylinders, the ankle joint package size is reduced significantly (See Figure 28).

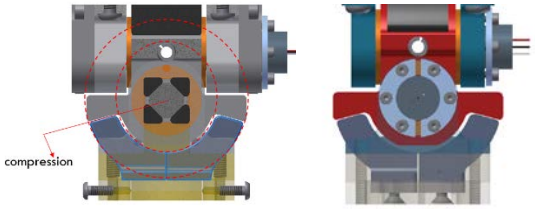

Figure 29: The redesigned THOR-05F ankle bumper with (left) and without (right) torque cylinders

Figure 30. Final ankle joint design without torque cylinders.

Friction Study

Friction between the rubber bumper and its compressing part was studied. Comparison between friction coefficients 0.3 and 0.6 shows that for the original design, there was little difference until about 25 degrees of rotation, at which point the response with higher friction increased in stiffness relative to that with lower friction (See Figure 29). For the final design, no difference was observed through the whole range of motion (See Figure 30). Most likely, in the original design, when the bumper bottoms out, the contact area increased and caused the noticeable change in result. Because the final

design eliminated the high local stress, the friction contribution was insignificant and consistent throughout the range of motion.

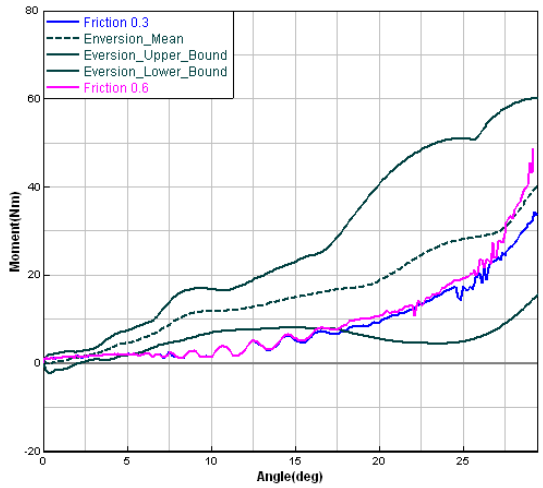

Figure 31. Friction study for original design with friction coefficients 0.3 and 0.6.

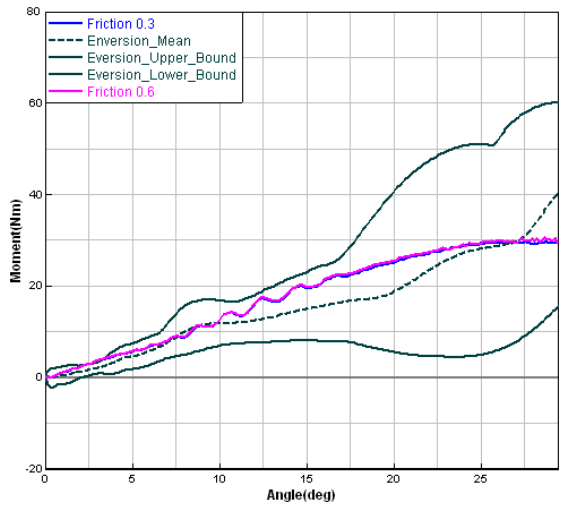

Figure 32. Friction study for the final design with friction coefficients 0.3 and 0.6.

Material Stiffness Study

Using the final ankle joint design, two rubber materials with different stiffness were analyzed with FE (See Figure 33).

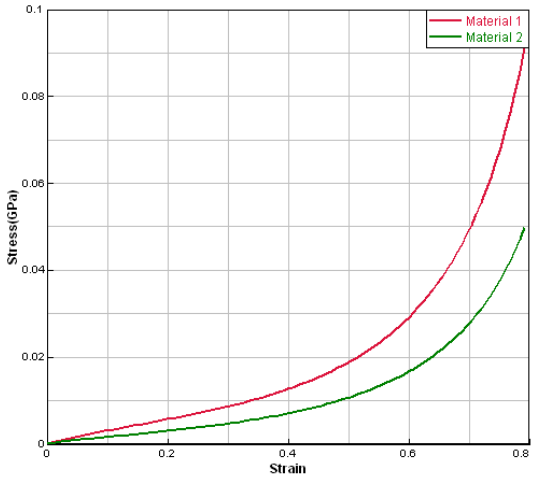

Figure 33. Rubber material properties for stiffness sensitivity FE analysis

The eversion responses are above and below the biomechanical response requirements (See Figure 32), demonstrating the ability to tune the response to meet biofidelity specifications. The response in inversion, which is less stiff than the eversion response, was less sensitive to the materials stiffness change (See Figure 33). The final material stiffness will be adjusted and determined in prototype testing.

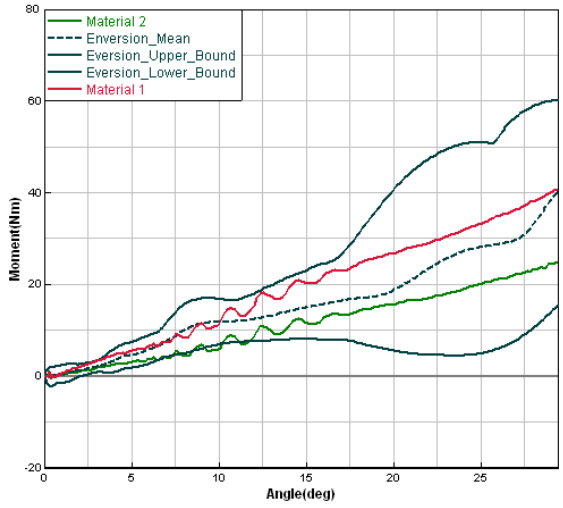

Figure 34. Inversion responses of the final ankle joint design with different material stiffness

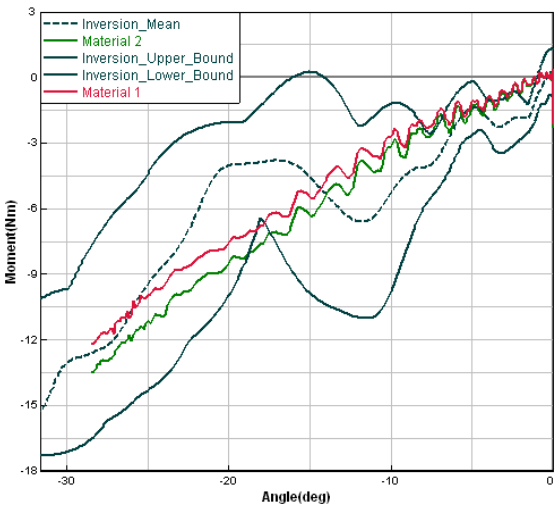

Figure 35. Eversion of the final ankle joint design with different material stiffness

Mass, Center of Gravity and Mass of Moment Inertia

The mass and center of gravity of the THOR-05F were designed to match the UMTRI AMVO 5th percentile female specifications. The details are summarized in Appendix 1. Each segment mass was calculated in CAD in accordance with the UMTRI AMVO body segmentation planes. ATD parts were cut virtually in CAD in order to allow comparison with UMTRI AMVO 5th female specifications. This is for design purpose only and cannot be realized in actual ATD parts without cutting the physical dummy part.

THOR-05F design can be configured with up to 168 instrumentation channels (see Appendix 2 for available instrumentation). The design incorporates 15 load cells. The facial load cell, femur load cell and Achilles load cells are shared with THOR-50M and the remaining 12 load cells are new designs. The load cell capacity is summarized in Appendix 2.

In-dummy data acquisition system (DAS) was taken into consideration in design. Structural replacements for all DAS and related electronics were implemented in ATD design, along with necessary cavities for cable routing.

The testing and evaluation plan includes 24 different tests for biofidelity, which include pendulum, linear impactor, quasi-static and sled tests. The biofidelity tests are summarized in Table 15 of Appendix 3. The biofidelity ranking (BioRank) will be calculated according to Rhule et al 2013. The biofidelity requirement is to achieve a BioRank score of 2.0 or less for each body region (head, neck, thorax, shoulder, abdomen, knee/thigh/hip, lower leg). First, the BioRank score will be calculated for each required response measurement. Then for each test condition, the BioRank scores for the required response measurements will be averaged to obtain a Test Condition BioRank score (TCBR score). For each body region, the TCBR scores will then be averaged to obtain a Body Region BioRank score (BRBR score). Criteria are also divided into primary and secondary specifications. Primary specifications must be met according to the BioRank or alternative requirements.

Qualification tests are to be developed starting from the THOR-50M qualification procedures, with modifications as necessary to account for geometry and instrumentation unique to the THOR-05F design. The evaluation results will be analyzed and presented in the future.

CONCLUSIONS

The THOR-05F ATD was designed to represent a 5th percentile female occupant for vehicle safety development. The design used the same concepts as THOR-50M to keep the similarity of the design as part of the THOR ATD family. Changes were incorporated from lessons learned in the development and implementation of the THOR-50M, plus female-specific body

features. Unique features of the THOR-05F design include combined skull and facial load cell mounting plate, integrated sternum-breast design to improve breast position accuracy, spine adjustment joint range of motion limiter, abdomen pressure twin sensors to replace abdomen IR-TRACCs, female-specific pelvic bone geometry, redesigned ankle joint to improve durability and repeatability, human-like metatarsal representation in foot design, humerus offset at the shoulder joint , and many other small items related to assembly and handling. The design was released for prototyping to evaluate the durability and biofidelity. The evaluation results will be presented in the future.

ACKNOWLEDGEMENT

The project is funded by NHTSA contract DTNH22-13-D-00301. The views presented in this paper are these of the authors and do not necessary reflect those of their respective organizations.

REFERENCES

Bose, D., Segui-Gomez, M., and Crandall, J., 2011. Vulnerability of female drivers involved in motor vehicle crashes: An analysis of US population at risk. Am J Public Health, 101, pp. 2368-2373.

EEVC Report – Advanced child dummies and injury criteria for frontal impact, January 2016.

Funk, J.R., Srinivasan. S.M., Crandall,J.R., Khaewpong,N., Eppinger, R.H., Jaffredo, A.S., Potier, P., Petit, P.Y., 2002. The effects of axial preload and dorsiflexion on the tolerance of the ankle/subtalar joint to dynamic inversion and eversion, Stapp Car Crash Journal, vol. 46, pp. 245-265.

Gordon, C.C., Churchill, T., Clauser, C.E., Bradtmiller, B., McConville, J.T., Tebbetts, I., Walker, R.A., 1988. Anthropometric survey of US Army personnel: methods and summary statistics. Technical Report NATICK/TR-89/044.

Kahane, C.J., 2013. Injury vulnerability and effectiveness of occupant protection technologies for older occupants and women. Report No. DOT HS 811 766. Washington, DC: National Highway Traffic Safety Administration.

Kent, R, Lee, H., Darvish, K., Wang, S., Poster, C.S., Lange, A.W., Brede, C. and Lange, D., 2005. Structural and material changes in the aging thorax and their role in crash protection for older occupants, Stapp Car Crash Journal, Vol. 49, pp. 231-249.

Klein, K.F., Reed, M.P. and Rupp, J.D., 2016a. Development of geometric specifications for the pelvis of a small female anthropometric test device, IRCOBI Conference Proceedings, Malaga, Spain. September 14-16.

Klein, K.F., Reed, M.P. and Rupp, J.D., 2016b. Development of geometric specifications for the pelvis of a small female anthropometric test device, Report No. DOT HS 812 339. Washington, DC: National Highway Traffic Safety Administration.

Lemmen, P., Been, B., Carroll, J. Hynd, D. Davidsson, J., Martinez, L. Garcia A., Vezin, P., Eggers, A., 2013. An advanced thorax-shoulder design for the THOR dummy, 23rd ESV Conference Proceedings, Republic of Korea.

Lu, Y.C., Untaroiu, C.D., 2013. Statistical shape analysis of clavicular cortical bone with applications to the development of mean and boundary shape models, Computer Methods and Programs in Biomedicine, Issue 11, pp. 613-628.

Martin, P.G., Craig, M., Ridella, S., Rigby, P., Chan, P. 2009. OOP Air bag tests with the fifth percentile female THOR and Hybrid III dummies, 21st ESV, Stuttgart, Germany, June 15-18.

McDonald, J.P., Shams, T., Rangarajan, N., and Beach, D. 2003. Design and development of a THOR based small female crash test dummy. Stapp Car Crash Journal, 47, pp. 551.

Parenteau, C.S., Zuby, D., Brolin, K.B., et al. 2013. Restrained male and female occupants in frontal crashes: Are we different? Proceedings of the International Research Council on Biomechanics of Injury (IRCOBI) Conference. Paper # IRC-13-98.

Reed, M.P. and Rupp, J.D., 2013. An Anthropometric comparison of current ATDs with the U.S. adult population, Traffic Injury Prevention, Vol. 14, Issue 7, pp. 703-705.

Rhule, H., Donnelly, B., Moorhouse, K., Kang, Y.S., 2013. A methodology for generating objective targets for quantitatively assessing the biofidelity of the crash test dummies, 23rd ESV, Seoul, Korea, May 27-30.

Robbins, D.H., 1983. Anthropometric specifications for small female and large male dummies, Volume 3, Technical Report UMTRI-83-53-3.

Shams, R., Beach, D., Huang, T., Rangaranjan, N., and Haffner, M., 2002. Development of THOR-Flx: a biofidelic lower extremity for use with 5th percentile female crash test dummies. Stapp Car Crash Journal, Vol 46, pp.267-283.

Tylko, S., Charlebois, D., 2006. The effect of breast anthropometry on the Hybrid III 5th female chest response, Stapp Car Crash Journal, Vol. 50, pp. 389-414.

Appendix 1 Mass, Center of Gravity and Mass Moment of Inertia

The body segment mass is shown in Table 2. As mentioned before, the segment planes correspond to that in UMTRI AMVO 5th percentile female. It is not applicable to the physical dummy unless the physical dummy parts are sectioned.

Table 2: THOR-05F body segment mass

Body Segment	UMTRI AMVO 5th	THOR-05F
Head (kg)	3.70	3.72
Neck (kg)	0.6	0.765
Thorax (kg)	12.98	12.54
Abdomen (kg)	1.61	1.61
Pelvis (kg)	6.98	6.61
Upper Arm	1.12	1.12
Forearm and	1.14	1.14
Upper leg (kg)	5.91	5.91
Lower leg (kg)	2.36	2.36
Foot [i] (kg)	0.64	1.07
Shoe [ii] (kg)	0.37	
Jacket [iii] (kg)		0.64
Total (kg)	48.95	49.09

[i] UMTRI is barefoot, CAD Design has the foot and shoe combined.
[ii] Shoe mass was derived from scaling of THOR-50M molded foot and shoe, not an UMTRI Specification.
[iii] Estimated from SID-IIs jacket mass.

The head mass, CG and MOI are summarized in Table 3. The components included in calculation in CAD is shown in Figure 34.

Table 3. THOR-05F head mechanical properties

Head Assembly	UMTRI AMVO 5th	THOR-05F
Mass (kg)	3.70	3.72
Head Length, L (cm)	18.3	18.4
Head Breadth, B (cm)	14.5	14.68
Head Height, H (cm)	20	20
CG, relative to OC, x (mm)	5	6.5
CG, relative to OC, z (mm)	59	54.7
Segment MOI, Ixx (kg-cm^2)	146.2	147.6
Segment MOI, Iyy (kg-cm^2)	172.9	162.5
Segment MOI, Izz (kg-cm^2)	131.7	101.9

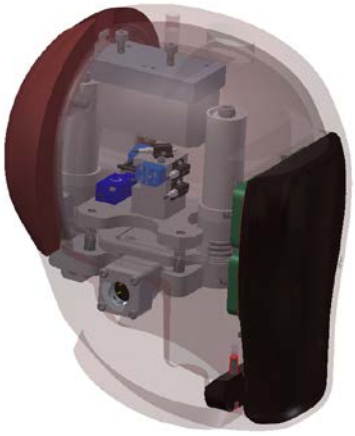

Figure 36. Parts included in head mechanical property calculation

The neck mass, CG and MOI are summarized in Table 4 and the parts included in the calculation is in Figure 35.

Table 4. Mechanical properties of the neck

	UMTRI AMVO 5TH	THOR-05F
Mass (kg)	0.6	0.765
CG, relative to OC, x (cm)	-17	-5.8
CG, relative to OC, z (cm)	-59	-45.4
Segment MOI, Ixx (kg-cm2)	6.1	17.8
Segment MOI, Iyy (kg-cm2)	9.5	19
Segment MOI, Izz (kg-cm2)	10.3	3.5

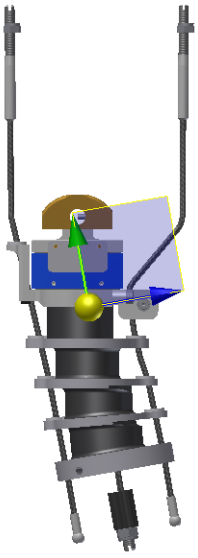

Figure 37. Parts included in neck mass, CG and MOI calculation

The thorax mass, CG and MOI are summarized in Table 5 and the parts included in the calculation is shown in Figure 36.

Table 5. Mass, CG and MOI of THOR-05F thorax

Thorax	UMTRI AMVO 5TH	THOR-05F
Mass (kg)	12.98	12.97*
CG, relative to hip, x (mm)	-147	-174.7
CG, relative to hip, z (mm)	238	267
Segment MOI, I_{xx} (kg-cm^2)	1542.8	927
Segment MOI, I_{yy} (kg-cm^2)	1161.2	486
Segment MOI, I_{zz} (kg-cm^2)	1208.6	540

* The dummy thorax mass without the jacket is 12.54 kg. The portion of the jacket mass, 0.43 kg was estimated and added to calculate the total thorax mass. Jacket are not included in the calculation of other specifications, i.e. CGs and MOIs.

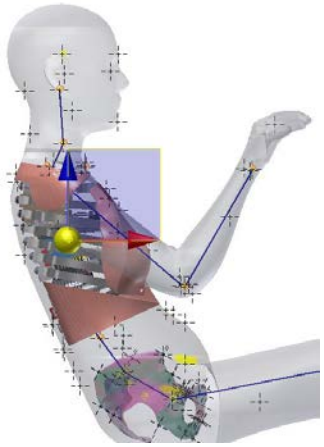

Figure 38. Parts included in thorax mechanical properties calculation

The upper abdomen mass, CG and MOI are summarized in Table 6 and the parts included in calculation are shown in Figure 37.

Table 6. Mass, CG and MOI of THOR-05F abdomen

	UMTRI AMVO 5TH	THOR-05F
Mass (kg)	1.61	1.61
CG, relative to hip, x (mm)	-82	-75
CG, relative to hip, z (mm)	107	102
Segment MOI, I_{xx} (kg-cm^2)	143.5	81.3
Segment MOI, I_{yy} (kg-cm^2)	101.5	57.8
Segment MOI, I_{zz} (kg-cm^2)	205.7	124.2

*Abdomen density 0.64 gram/cc was used for calculation.

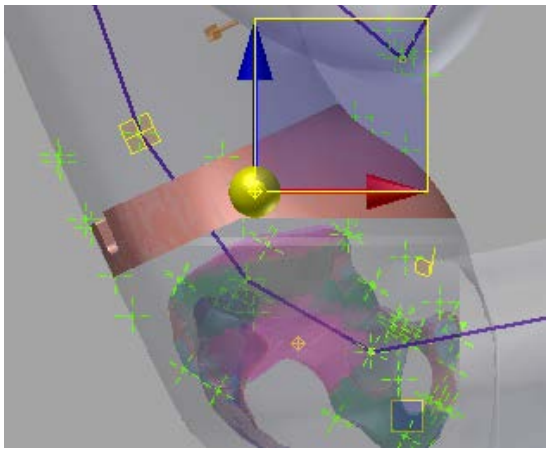

Figure 39, THOR-05F abdomen segmentation planes

The pelvis mass, CG and MOI are summarized in Table 7 and the parts included in the calculation are shown in Figure 38.

Table 7. Mass, CG and MOI for THOR-05F Pelvis.

	UMTRI AMVO 5TH	THOR-05F
Mass (kg)*	6.98	6.82
CG, relative to hip, x (mm)	-76	-45
CG, relative to hip, z (mm)	25	8.7
Segment MOI, I_{xx} (kg-cm²)	326.2	333.7
Segment MOI, I_{yy} (kg-cm²)	282.9	232.9
Segment MOI, I_{zz} (kg-cm²)	574.2	382.4

Note: Mass includes jacket. All other values (CG, MOI) are without jacket. Final design without jacket 6.61 kg. Lower abdomen density is 0.29 g/cc, 1/3 SID-IIs jacket mass is 0.64 kg, i.e. 0.21 kg, is included for pelvis mass.

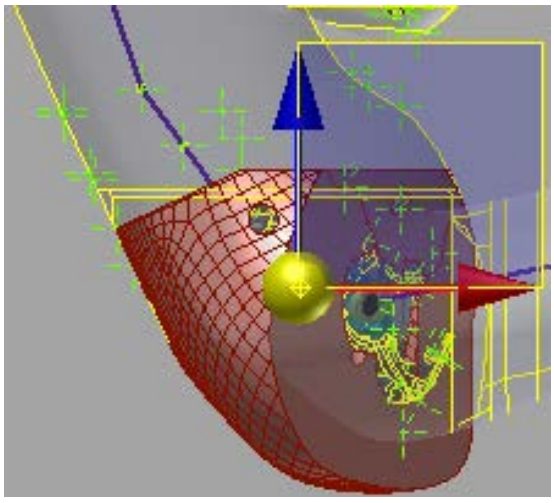

Figure 40. THOR-05F pelvis segmentation for mass, CG and MOI

The upper arm mass, CG and MOI are summarized in Table 8. The parts included in the calculation are shown in Figure 39.

Table 8. Mass, CG and MOI of THOR-05F upper arm.

	UMTRI AMVO 5TH	THOR-05F
Mass (kg)	1.12	1.12
CG, relative to Elbow (mm)	145.1	141.2
Segment MOI, I_{xx} (kg-cm^2)	50	51.8
Segment MOI, I_{yy} (kg-cm^2)	51.1	52.9
Segment MOI, I_{zz} (kg-cm^2)	8.2	5.2

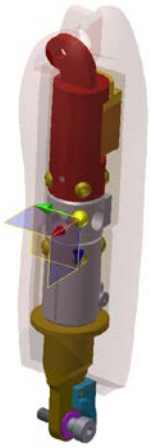

Figure 41. Parts included in mass, CG and MOI calculation of THOR-05F upper arm

The mass, CG and MOI of the forearm and hand are summarized in Table 9. The parts included in the calculation are shown in Figure 40.

Table 9. Mass, CG and MOI of THOR-05F forearm and hand

Lower Arm Assembly	UMTRI AMVO 5TH	THOR-05F
Mass (kg)	1.14	1.14
CG, relative to Elbow (mm)	140.9	141.2
Segment MOI, I_{xx} (kg-cm^2)	141.5	117.7
Segment MOI, I_{yy} (kg-cm^2)	129.4	116.5
Segment MOI, I_{zz} (kg-cm^2)	8.3	4.9

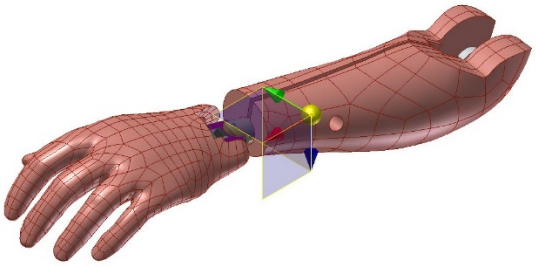

Figure 42. Parts included for mass, CG and MOI for THOR-05F forearm and hand

The upper leg mass, CG and MOI are summarized in Table 10. The parts included in the calculation are shown in Figure 41.

Table 10. Mass, CG and MOI of THOR-05F upper leg

	UMTRI AMVO 5TH	**THOR-05F**
Mass (kg)	5.91	5.91
CG, relative to hip (mm)	149	187
Segment MOI, Ix (kg-cm^2)	153.9	120.1
Segment MOI, Iy (kg-cm^2)	701	665
Segment MOI, Iz (kg-cm^2)	731.4	646.6

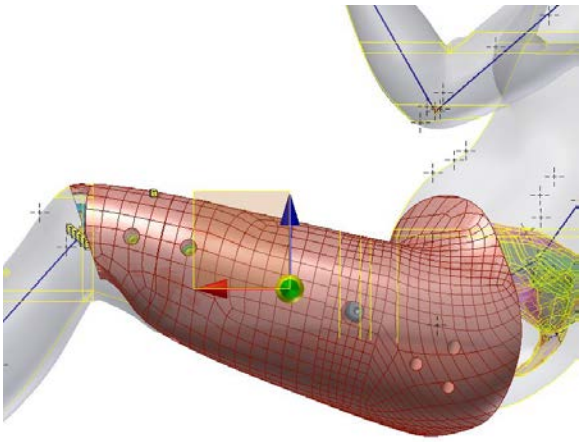

Figure 43. Segmentation for THOR-05F upper leg

The lower leg mass, CG and MOI are summarized in Table 11. The parts included in the calculation are shown in Figure 42.

Table 11. Mass, CG and MOI of THOR-05F lower leg

	UMTRI AMVO 5TH	THOR-05F
Mass (kg)	2.36	2.36
CG, relative to knee (mm)	150.8	157.9
Segment MOI, Ix (kg-cm^2)	261.4	216.3
Segment MOI, Iy (kg-cm^2)	261.9	213.0
Segment MOI, Iz (kg-cm^2)	23.1	21.3

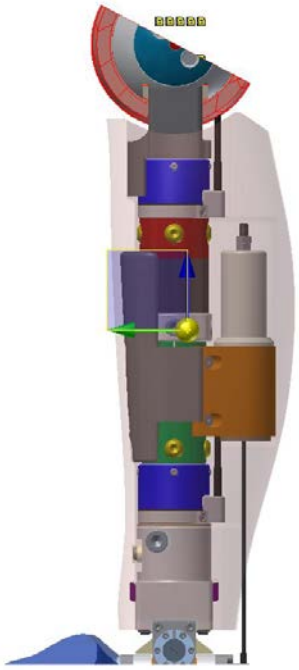

Figure 44. Segmentation of THOR-05F lower leg

The foot mass, CG and MOI calculated from CAD are summarized in Table 12. The parts included in the calculation are shown in Figure 43. For the proposed spec of the molded shoe, a shoe specification was added to the UMTRI AMVO foot mass target (0.64 kg). The specification for the 50th MIL-spec shoe, according to CFR 571.208 is a weight of 1.25 ±0.2 lb. (0.567 ± 0.091 kg). Mass for the 5th MIL-spec shoe is not specified in CFR 571.208. However, assuming the shoe weight will scale by the same mass ratio as the foot mass, the target 5th shoe weight would be 0.37 ± 0.13 kg.

Table 12. Mass, CG and MOI of THOR-05F molded shoe and foot

Specification	**UMTRI AMVO (Bare foot)**	**Proposed 5TH SPEC (Foot + Molded Shoe)**	**THOR-05F**
Mass (kg)	0.64	0.95-1.07	1.126
CG, relative to Heel (mm)	84	NA	75.1
Segment MOI, Ix (kg-cm^2)	3.4	NA	10.4
Segment MOI, Iy (kg-cm^2)	18.4	NA	49.6

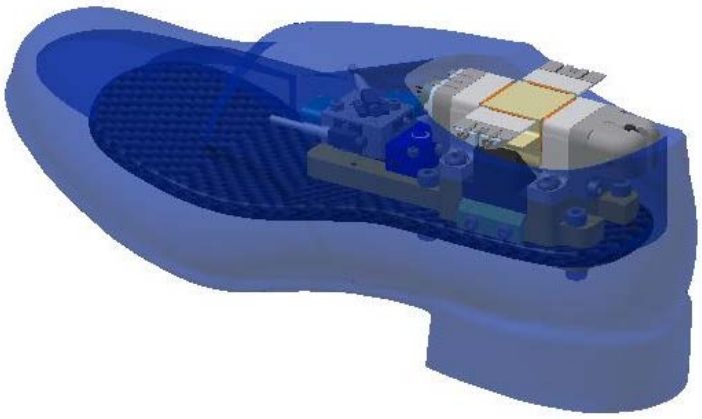

Figure 45. Segmentation of THOR-05F foot

Appendix 2 THOR-05F Full Channel Counts and Load Cell Capacity

The channel list for THOR-05F is summarized in Table 13.

Table 13. THOR-05F available instrumentation

Description	Sensor Type	Channels	Channel Per Sensor	QTY	Subtotal Channel
Head CG accelerometers	accelerometer	Ax, Ay, Az	1	3	3
Head CG accelerometers - redundant	accelerometer	Ax, Ay, Az	1	3	3
Head angular rate sensor	ARS	ωx, ωy, ωz	1	3	3
Facial load cell	load cell	Fx	1	5	5
Neck spring load cell	load cell	Fz	1	2	2
Upper neck load cell	load cell	Fx, Fy, Fz, Mx, My, Mz	6	1	6
Lower neck load cell	load cell	Fx, Fy, Fz, Mx, My, Mz	6	1	6
OC rotary pot	potentiometer	θy	1	1	1
Clavicle load cell, left	load cell	Fx, Fz (medial, Lateral)	4	1	4
Clavicle load cell, right	load cell	Fx, Fz (medial, Lateral)	4	1	4
T1 linear accelerometers	accelerometer	Ax, Ay, Az	1	3	3
Mid sternum Accelerometers	accelerometer	Ax	1	1	1
Thoracic IR-TRACC upper left	IR-TRACC	Dx	1	1	1
Rotary pot - IR-TRACC UL	potentiometer	θy	1	1	1
Rotary pot - IR-TRACC UL	potentiometer	θz	1	1	1
Thoracic IR-TRACC upper right	IR-TRACC	Dx	1	1	1
Rotary pot - IR-TRACC UR	potentiometer	θy	1	1	1
Rotary pot - IR-TRACC UR	potentiometer	θz	1	1	1
Thoracic IR-TRACC lower left	IR-TRACC	Dx	1	1	1
Rotary pot - IR-TRACC LL	potentiometer	θy	1	1	1
Rotary pot - IR-TRACC LL	potentiometer	θz	1	1	1
Thoracic IR-TRACC lower right	IR-TRACC	Dx	1	1	1
Rotary pot - IR-TRACC LR	potentiometer	θy	1	1	1
Rotary pot - IR-TRACC LR	potentiometer	θz	1	1	1
T8 accelerometers	accelerometer	Ax, Ay, Az	1	3	3
Thoracic spine load cell (T12)	load cell	Fx, Fy, Fz, Mx, My, Mz	6	1	6
Thorax angular rate sensor (T12)	ARS	ωx, ωy, ωz	1	3	3
T12 accelerometers	accelerometer	Ax, Ay, Az	1	3	3
Abdomen pressure sensor	APTS	P	1	2	2

Pelvis CG accelerometers	accelerometer	Ax, Ay, Az	1	3	3
Pelvis CG ARS	ARS	ωx, ωy, ωz	1	3	3
Acetabular load cell, left	load cell	Fx, Fy, Fz	3	1	3
Acetabular load cell, right	load cell	Fx, Fy, Fz	3	1	3
ASIS load cell, left	load cell	Fx, My	2	1	2
ASIS load cell, right	load cell	Fx, My	2	1	2
Femur load cell, L&R	load cell	Fx, Fy, Fz, Mx, My, Mz	6	2	12
Knee potentiometer, left	string pot	Dx	1	1	1
Knee potentiometer, right	string pot	Dx	1	1	1
Upper tibia load cell, L&R	load cell	Fx, Fy, Fz, Mx, My	5	2	10
Lower tibia load cell, L&R	load cell	Fx, Fy, Fz, Mx, My	5	2	10
Tibia accelerometers, left	accelerometer	Ax, Ay	1	2	2
Tibia accelerometers, right	accelerometer	Ax, Ay	1	2	2
Achilles load cell, L&R	load cell	Fz	1	2	2
Ankle rotation, left	pot	θx, θy, θz	1	3	3
Ankle rotation, right	pot	θx, θy, θz	1	3	3
Foot accelerometers, left	accelerometer	Ax, Ay, Az	1	3	3
Foot ARS, left	ARS	ωx, ωy, ωz	1	3	3
Foot accelerometers, right	accelerometer	Ax, Ay, Az	1	3	3
Foot ARS, right	ARS	ωx, ωy, ωz	1	3	3
Upper arm load cell, L&R	load cell	Fx, Fy, Fz, Mx, My, Mz	6	2	12
Lower arm load cell, left	load cell	Fx, Fy, Fz, Mx, My, Mz	6	1	6
Lower arm load cell, right	load cell	Fx, Fy, Fz, Mx, My, Mz	6	1	6
Total					168

The load cell of THOR-05F is summarized in Table 14.

Table 14: THOR-05F capacities of available instrumentation

Description	**Fx (KN)**	**Fy (KN)**	**Fz (KN)**	**Mx (Nm)**	**My (Nm)**	**Mz (Nm)**
Facial load cell	4,500	NA	NA	NA	NA	NA
Upper neck load cell	6,700	6,700	10,000	210	210	135
Lower neck load cell	10,000	10,000	12,000	300	300	200
Clavicle load cell, left	2,000	NA	2,000	NA	NA	NA
Clavicle load cell, right	2,000	NA	2,000	NA	NA	NA
Upper arm, left & right	9,000	9,000	13,500	190	190	170
Lower arm, left & right	9,000	9,000	13,000	190	190	170
Thoracic Spine load cell	13,000	13,000	13,000	560	560	280
Acetabulum load cell, left	13,000	9,000	9,000	NA	NA	NA
Acetabulum load cell, right	13,000	9,000	9,000	NA	NA	NA
ASIS load cell, left & right	13,000	NA	NA	NA	200	NA
Femur load cell, left & right	9,000	9,000	13,500	225	225	170
Upper tibia, left & right	10,000	10,000	12.,000	340	340	NA
Lower tibia, left & right	10,000	10,000	12,000	340	340	NA
Achilles load cell, left & right	NA	NA	4,450	NA	NA	NA

Appendix 3 Biofidelity Test and References

Table 15 List of biofidelity tests for THOR-05F

Item #	Body Region	Description	Reference	Biofidelity Specifications	Priority
1	Head Test 1	Pendulum	Melvin et al 1985	Head Pendulum Impact - 2.0 m/s	primary
2	Head Test 2	Pendulum	Nyquist et al 1986	Round Rigid Bar impact (Face)	primary
3	Head Test 3	Pendulum	Melvin & Shee, 1989	Rigid Disk impact (Face)	primary
4	Neck Test 1	Sled	Thunnissen et al 1995	Frontal Flexion-kinematic	primary
5	Neck Test 2	Pendulum	Mertz & Patrick, 1971	Frontal flexion-dynamic	secondary
6	Neck Test 3	Sled	Wismans and Spenny, 1984	Lateral Flexion-kinematic	primary
7	Neck Test 4	Pendulum	Patrick & Chou, 1976	Lateral flexion-dynamic	secondary
8	Neck Test 5	Pendulum	Myers et al 1991	Torsional Load-dynamic	primary
9	Thorax Test 1	Pendulum	Kroell et al 1974; Neathery et al 1974	Upper central ribcage impact - 4.3 m/s	primary
10	Thorax Test 2	Pendulum	Kroell et al 1974; Neathery et al 1974	Upper central ribcage impact - 6.7 m/s	durability test
11	Thorax Test 3	Pendulum	Yoganandan et al 1997	Lower oblique impact	primary
12	Thorax & Shoulder Test	Sled	Shaw et al 2009 / unpublished 5th data	Sled test (Gold Standard)	secondary
13	Shoulder Test	Quasi-static	Tornvall et al 2005	Shoulder Range of Motion/ Stiffness	primary
14	Abdomen Test 1	Pendulum	Cavanaugh et al 1986	Lower L3 rigid bar, 32 kg - 6.1 m/s	primary
15	Abdomen Test 2	Pendulum	Nusholtz et al 1994	Upper Abdomen steering wheel rim, 20 degree from vertical 18 kg - 6.7 m/s	primary
16	Abdomen Test 3	Quasi-static	Lamielle et al 2008	Belt loading (unspecified)	secondary
17	Lumbar Test	Pendulum	Parent, unpublished	Lumbar Pendulum Test	primary
18	Knee/Thigh/Hip Test 1	Linear impactor	Rupp et al 2008	Femur impact, 255 kg, whole body - 4.9 m/s	primary
19	Knee/Thigh/Hip Test 2	Linear impactor	Rupp et al 2003	Femur (lower extremity isolated) impact, 250 kg - 1.2 m/s	primary
20	Knee/Thigh/Hip Test 3	Pendulum	Balasubramanian et al 2004	Knee slider - 2.75 m/s	primary
21	Leg Test 1 - Heel	Pendulum	Funk et al 2000	Tibia axial, 20 kg - 7 m/s	primary
22	Leg Test 2 - Ball	Pendulum	Crandall et al 1996	Dorsiflexion dynamic - 5.0 m/s	primary

23	Leg Test 3 - Inversion	Pendulum	Funk et al 2002	Dynamic Inversion/eversion, neutral position	primary
24	Leg Test 4 - Eversion	Pendulum	Funk et al 2002	Dynamic Inversion/eversion, neutral position	primary

Biofidelity Test References

Balasubramanian, S., Beillas, P., Belwadi, A., Hardy, W.N., Yang, K.H., King, A.I., Masuda, M., 2004. Below knee impact responses using cadaveric specimens, Stapp Car Crash Journal, Vol. 48, pp. 71-88.

Crandall, J.R., Portier, L., Petit, P., Hall, G.W., Bass,C.R., Klopp,G.S., Hurwitz, S., Pilkey, W.D., Trosseille, X., Tarriere, C., Lassau, J.P., 1996, Biomechanical response and physical properties of the leg, foot and ankle, 40th Stapp Car Crash Conference, Albuquerque, New Mexico.

Cavanaugh, J., Nyquist, G., Goldberg, S., and King, A. 1986. Lower abdominal tolerance and THOR-05F Biomechanical Response Requirements. Proceedings of the 30th Stapp Car Crash Conference. SAE Technical Paper # 861878.

Funk, J.R., Tourret L.J., Crandall J.R. 2000. Experimentally produced tibial plateau fractures. International IRCOBI Conference on the Biomechanics of Impact, pp 171-182.

Funk, J.R., Srinivasan. S.M., Crandall,J.R., Khaewpong,N., Eppinger, R.H., Jaffredo, A.S., Potier, P., Petit, P.Y., 2002. The effects of axial preload and dorsiflexion on the tolerance of the ankle/subtalar joint to dynamic inversion and eversion, Stapp Car Crash Journal, vol. 46, pp. 245-265.

Kroell, C.K. and Schneider, D.C. and Hahum, A.M., 1974. Impact tolerance and response of human thorax II, 18th Stapp Car Crash Conference Proceeding.

Lamielle, S., Vezin, P., Verriest, J.P., Petit, P., et al. 2008. 3D Deformation and dynamics of the human cadaver abdomen under seatbelt loading. Stapp Car Crash Journal, Vol. 50. SAE Paper # 2008-22-0011.

Melvin, J.W., 1985, The engineering design, development, testing and evaluation of an Advanced Anthropomophic Testing Device (AATD), Phase I: Concept Definition – Executive Summary.

Melvin, J., and Shee, T. 1989. Facial Injury Assessment Techniques. Proceedings of the 12th International Conference on Experimental Safety Vehicles (ESV).

Mertz, H.J. and Patrick, L.M., 1971. Strength and response of the human neck, 15th Stapp Car Crash Conference, San Diego, California.

Myers, B.S., McElhaney, J.H., Doherty, B.J., Paver, J.G. and Gray L., 1991. The role of torsion in cervical spine trauma, SPINE, Vol 16, No. 6.

Neathery, R., 1974. Analysis of Chest Impact Response Data and Scaled Performance Recommendations, 18th Stapp Car Crash Conference. SAE Technical Paper 741188.

Nusholtz, G., and Kaiker, P. 1994. Abdominal response to steering wheel loading. Proceedings of the 14th International Conference on Experimental Safety Vehicles. p. 118-27.

Nyquist, G., Cavanaugh, J., Goldberg, S., and King, A. 1986. Facial Impact Tolerance and Response. Proceedings of the 30th Stapp Car Crash Conference.

Patrick, L.M., Chou, C.C., 1976. Response of the human neck in flexion, extension and lateral flexion. Vehicle Institute Report No. VRI-7.3. Society of Automotive Engineers, Warrendale, PA.

Rupp, J.D., Miller, C.S., Reed, M.P., Madura, N.H., Klinich, K. and Schneider, L., 2008. Characterization of knee-thigh-hip response in frontal impacts using biomechanical testing and computational simulations, Stapp Car Crash Journal, Vol. 52, pp. 421-474.

Rupp, J.D., Reed, M.P., Madura, N.H., Miller, C.S., Kuppa, S., 2005. Comparison of the inertial response of the THOR-NT, Hybrid III, and unembalmed cadaver to simulated knee-to-knee-boster impacts, 19th International Technical Conference on the Enhanced Safety of Vehicles, Washington DC.

Shaw, G., Parent, D., Purtsezov, S., Lessley, D., Crandall, J., Kent, R., Guillemot, H., Ridella, S., Takhounts, E. and Martin, P., 2009. Impact response of restrained PMHS in frontal sled tests: skeletal deformation patterns under seat belt loading. Stapp Car Crash Journal, Vol. 53, pp1-48.

Thunissen, J., Wismans, J.. Ewing, C.L., Thomas D.J..1995. Human Volunteer Head-Neck Response in Frontal Flexion: A New Analysis. Thirty-ninth Stapp Car Crash Conference, San Diego, California, November 8-10, SAE Paper # 952721.

Törnvall, F.V., Holmqvist, K, Martisson, J. and Davidsson, J. 2005. Comparison of shoulder range of motion and stiffness between volunteers, Hybrid III and THOR alpha in static frontal impact loading, International Journal of Crashworthiness, Vol 10, No. 2, pp 151-160.

Wismans, J. and Spenny, C.H., 1983, Performance requirements for mechanical necks in lateral flexion, Proceedings of 27th Stapp Car Crash Conference, SAE paper No. 831613, Warrendale, PA 15096, pp137-148.

Yoganandan, N., Pintar, F., Kumaresan, S., 1997. Impact biomechanics of the human thorax-abdomen complex. International Journal of Crash, Vol 2, No. 2, pp 219-228.